modelling

MDPI

Article

Modeling the Bending of a Bi-Layer Cantilever with Shape Memory Controlled by Magnetic Field and Temperature

Olga S. Stolbova * and Oleg V. Stolbov

Institute of Continuous Media Mechanics, Russian Academy of Sciences, Ural Branch, Perm 614018, Russia; sov@icmm.ru

* Correspondence: sos@icmm.ru

Abstract: This paper presents a model of the bending behavior of a bi-layer cantilever composed of titanium nickelide and a magnetoactive elastomer embedded with magnetically hard particles. The cantilever is initially subjected to an external magnetic field in its high-temperature state, followed by cooling to a low-temperature state before the magnetic field is removed. This sequence results in residual bending deformation. Basic relations describing the material behavior of titanium nickelide and the magnetoactive elastomer are presented. A variational formulation for the problem under consideration is written down. The problem is solved numerically using the finite element method. The influence of the applied magnetic field magnitude and the thickness of the titanium nickelide layer on the cantilever deflection magnitude is studied. The dependence of the residual cantilever deflection on the applied magnetic field is obtained. The possibility of this structure as a controllable gripping element for applications in robotics and micro-manipulation is demonstrated.

Keywords: shape memory alloy; magnetoactive elastomer; bi-layer cantilever; numerical modeling; finite element method

Citation: Stolbova, O.S.; Stolbov, O.V. Modeling the Bending of a Bi-Layer Cantilever with Shape Memory Controlled by Magnetic Field and Temperature. *Modelling* **2024**, *5*, 1924–1935. https://doi.org/10.3390/modelling5040100

Academic Editors: Paolo Todisco and Elide Nastri

Received: 1 November 2024
Revised: 2 December 2024
Accepted: 3 December 2024
Published: 5 December 2024

1. Introduction

Actuators and grippers developed using functional materials have attracted significant attention in recent years due to their adaptability and ability to undergo complex deformations. These devices play a crucial role in robotics, medical manipulators, and microelectromechanical systems, offering the flexibility and control that traditional materials cannot provide [1–4]. Actuators made of various materials (shape memory alloys and polymers, magnetoactive and electroactive elastomers, etc.) are activated by various stimuli, such as thermal action, magnetic or electric fields [5–7]. Modern soft robotics technologies based on the use of functional materials significantly expand the possibilities of using different types of actuators and grippers [8–10].

Shape memory alloys, such as titanium nickelide, are often used to create actuators capable of changing shape when heated and returning to their original state when cooled [11,12]. Magnetoactive elastomers can alter their stiffness and shape under the influence of a magnetic field, making them suitable for adaptive grippers; grippers made from such materials are used for manipulating fragile objects as their softness and flexibility reduce the risk of damage [13,14]. Control by means of temperature and magnetic influence can be performed contactlessly. However, each of these influences has its own advantages and disadvantages. Temperature changes in the material typically occur more slowly than responses to magnetic fields. However, creating a magnetic field requires relatively bulky electromagnets or a permanent magnet with a positioning mechanism.

Traditional actuators often struggle to integrate dual-stimulus control, either relying solely on temperature or magnetic fields. The bi-layer system overcomes this limitation by enabling independent and combined control of deformation profiles. Combining SMA and MAE in a bi-layer configuration enables dual-stimuli actuation, where temperature

changes affect the SMA layer and magnetic fields affect the MAE layer, offering complex deformation capabilities compared to single-stimulus systems. To enable control of the actuator through both temperature and magnetic fields, we consider a bi-layer cantilever composed of a thermally activated shape memory alloy (specifically, titanium nickelide) and a magnetoactive elastomer containing magnetically hard NdFeB particles. To optimize the cantilever's deflection, we apply numerical modeling that takes into account the main mechanisms of strain accumulation in shape memory materials (alloys and polymers).

The deformation mechanism in shape memory alloys (SMAs), such as titanium nickelide NiTi (Nitinol), is based on the material's unique ability to recover its original shape with temperature changes. This effect is achieved due to the presence of two phases in these alloys: martensite and austenite. During cooling, a direct phase transformation from austenite to martensite occurs, and during heating, a reverse transformation from the martensitic state takes place. If the direct transformation occurs in an unstressed alloy, only a very small (approximately 0.3% for titanium nickelide) macroscopic volume deformation is observed, without shape change. However, if the direct transformation occurs under non-zero stress, macroscopic shape deformation accumulates during cooling; its deviator aligns with that of the applied stress, and its intensity in titanium nickelide can reach 8–10%. Upon heating and the corresponding reverse transformation, the accumulated deformation is removed, which is termed shape memory [15,16].

Magnetoactive elastomers (MAEs) are composite materials consisting of a polymer matrix and magnetic particles. MAEs filled with magnetically hard particles (such as NdFeB) can retain residual magnetization (in the absence of a magnetic field). When an external magnetic field is applied that is not aligned with the direction of residual magnetization, a torque arises that tends to align the magnetization along the magnetic field, causing macroscopic deformation of the sample. When the magnetic field is removed, the torque ceases to act and the sample returns to its initial shape [17]. The bending of cantilevers made from MAEs with magnetically hard particles can be effectively controlled by a magnetic field [18–21].

In [22], modeling of the bending of a bi-metallic plate of titanium nickelide and beryllium bronze, as well as a single-layer titanium nickelide plate, is presented. The plate is subjected to bending shear stresses at the end and cooled within the temperature range of the direct phase transition of the SMA. This study demonstrated that the thicknesses of the SMA and beryllium bronze layers influence the deflection of the bi-layer plate and determined the layer thickness ratio to achieve maximum plate deflection.

The article [23] is devoted to the development of an adaptive tuned vibration absorber, which uses a composition based on a magnetorheological elastomer (MRE) and a shape memory alloy (SMA). The material stiffness can be changed both by temperature (thanks to SMA) and magnetic field (thanks to MRE), providing a wider and smoother tuning range. The combined use of these materials allows the authors to eliminate the disadvantages of each of them separately and achieve a smooth and effective tuning of the system for vibration suppression.

In the present study, we model the behavior of a bi-layer cantilever composed of titanium nickelide and a magnetoactive elastomer containing NdFeB magnetically hard particles. An external magnetic field is applied to this cantilever in the high-temperature state, followed by cooling to a low-temperature state with subsequent removal of the magnetic field. The influence of various parameters on the cantilever deflection is investigated.

2. Materials and Methods

Consider a cantilever (bi-layer plate) composed of titanium nickelide and a magnetoactive elastomer containing magnetically hard NdFeB particles. The cross-section of such a plate is shown in Figure 1, with titanium nickelide shaded in red and the magnetoactive elastomer in blue. It is assumed that adhesion between the two layers is perfect (the displacement field is continuous). The plate has a length l (dimension along the x-axis) and a thickness h (dimension along the y-axis), with the titanium nickelide layer

thickness denoted by h_N and the magnetoactive elastomer layer thickness denoted by h_ε ($h = h_N + h_\varepsilon$). The plate is clamped at the left edge, while the other surfaces are free. Initially, the titanium nickelide layer is in the austenitic (high-temperature) state, and the magnetoactive elastomer has a residual magnetization $\mathbf{M}_r$, directed along the x-axis. An external magnetic field $\mathbf{H}_0$, directed along the y-axis, is applied to this sample, after which it is cooled to the martensitic (low-temperature) state of titanium nickelide, and the magnetic field is removed.

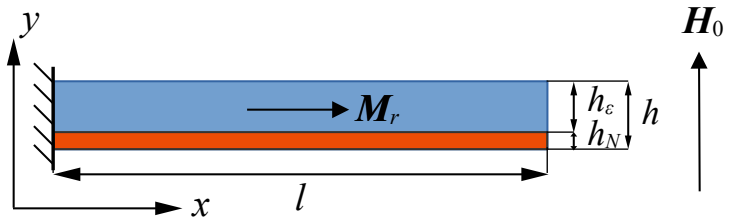

Figure 1. Cross-section of the bi-layer plate made of titanium nickelide (red area) and MAE (blue area).

To model the behavior of this bi-layer plate in the approximation of small deformations, the basic relations for the titanium nickelide layer and the magnetoactive elastomer are formulated, neglecting thermal deformations due to their minimal influence. During the cooling process, phase transformations will induce phase strains in the titanium nickelide that disappear upon subsequent heating. In the framework of small deformations, the additivity of elastic and phase strains is assumed.

2.1. Basic Relations for Titanium Nickelide

To describe the phase transition in shape memory alloys (SMAs), a scalar internal variable φ_M is introduced, representing the volume fraction of the martensitic phase in the material. This variable ranges from 0 in the fully austenitic (high-temperature) state to 1 in the fully martensitic (low-temperature) state. For a forward phase transition (austenite to martensite), the inequality $d\varphi_M > 0$ is valid, while for the reverse transition (martensite to austenite), $d\varphi_M < 0$ is satisfied. The phase transition diagram (the dependence of the martensitic phase fraction φ_M on temperature Θ) is approximated by the following relation (see, e.g., [22]):

$$\varphi_M(\xi) = \begin{cases} 0, & \xi \le 0, \\ 0.5\,(1 - \cos(\pi\,\xi)), & 0 < \xi < 1, \\ 1, & \xi \ge 1, \end{cases} \tag{1}$$

where

$$\xi = \frac{M_s^\sigma - \Theta}{M_s - M_f}, \quad M_f^\sigma \le \Theta \le M_s^\sigma \quad (d\varphi_M > 0);$$

$$\xi = 1 + \frac{A_s^\sigma - \Theta}{A_f - A_s}, \quad A_s^\sigma \le \Theta \le A_f^\sigma \quad (d\varphi_M < 0).$$

Here, M_s, M_f, A_s, and A_f are the start and finish temperatures of the forward and reverse martensitic transformations in the stress-free material, while M_s^σ, M_f^σ, A_s^σ, and A_f^σ are the start and finish temperatures of these transformations in the stressed material. Note that forward and reverse phase transitions occur at different temperatures: the temperature range $M_s \to M_f$ corresponds to the austenite-to-martensite transition, while $A_s \to A_f$ corresponds to the martensite-to-austenite transition.

For a stressed material, the critical transition temperatures are given by the following linear dependence on the stress intensity σ_i:

$$M_s^\sigma = M_s + \kappa\,\sigma_i, \quad M_f^\sigma = M_f + \kappa\,\sigma_i,$$
$$A_s^\sigma = A_s + \kappa\,\sigma_i, \quad A_f^\sigma = A_f + \kappa\,\sigma_i, \tag{2}$$

where κ is a material constant.

According to [24], the equations describing the evolution of phase strains are written as follows:

$$d\mathbf{e}_{Ph} = (\beta\,\mathbf{g} + c_0\,\mathbf{S} + a_0\,\mathbf{e}_{Ph})\,d\varphi_M, \quad d\varphi_M > 0, \tag{3}$$

$$d\mathbf{e}_{Ph} = \left(\frac{a_0\,\mathbf{e}_{Ph}^{(0)}}{\exp\left(a_0\,\varphi_M^{(0)}\right) - 1} + a_0\,\mathbf{e}_{Ph}\right) d\varphi_M, \quad d\varphi_M < 0. \tag{4}$$

Here, β, c_0, and a_0 are material parameters; $\mathbf{g}$ is the unit tensor; $d\mathbf{e}_{Ph}$ and $\mathbf{e}_{Ph}$ are the phase strain increment and current phase strain; $\varphi_M^{(0)}$ and $\mathbf{e}_{Ph}^{(0)}$ are the martensitic phase parameter and phase strain values at the initial point of the reverse transformation process; and $\mathbf{S}$ is the deviator of the stress tensor $\mathbf{T}$.

The elastic behavior of titanium nickelide is described by Hooke's law [25,26]:

$$\mathbf{T} = \lambda_N(\varphi_M)\,I_1(\mathbf{e}_E)\,\mathbf{g} + 2\,G_N(\varphi_M)\,\mathbf{e}_E, \tag{5}$$

where $\lambda_N(\varphi_M)$ and $G_N(\varphi_M)$ are the Lamé parameter and the shear modulus of titanium nickelide (their values change during the phase transition); $\mathbf{e}_E = \mathbf{e} - \mathbf{e}_{Ph}$ is the elastic strain tensor; $\mathbf{e}$ is the total strain tensor; and $I_1(\mathbf{e}_E)$ is the first invariant of $\mathbf{e}_E$.

The dependencies of the elastic properties of the material (Young's modulus $E_N(\varphi_M)$ and shear modulus $G_N(\varphi_M)$) on the martensitic phase fraction φ_M are defined by the following relations:

$$\frac{1}{E_N(\varphi_M)} = \frac{\varphi_M}{E_M} + \frac{1-\varphi_M}{E_A}, \qquad \frac{1}{G_N(\varphi_M)} = \frac{\varphi_M}{G_M} + \frac{1-\varphi_M}{G_A},$$

where E_M and G_M are the values of Young's modulus and shear modulus for the martensitic state, and E_A and G_A are the same values for the austenitic state. Hence, we obtain that

$$\lambda_N(\varphi_M) = \frac{E_N(\varphi_M) - 2\,G_N(\varphi_M)}{3\,G_N(\varphi_M) - E_N(\varphi_M)}\,G_N(\varphi_M).$$

2.2. Basic Relations for Magnetoactive Elastomer

The elastic behavior of the magnetoactive elastomer is also described by Hooke's law:

$$\mathbf{T} = \lambda_\varepsilon\,I_1(\mathbf{e})\,\mathbf{g} + 2\,G_\varepsilon\,\mathbf{e}, \tag{6}$$

where λ_ε and G_ε are the Lamé parameter and the shear modulus of the magnetoactive elastomer, and the elastic strains are equal to the total strains ($\mathbf{e}_E = \mathbf{e}$).

In the material under a magnetic field, a mass moment $\mathbf{L}_{mag} = \mu_0\,\mathbf{M}_r \times \mathbf{H}$ arises, where μ_0 is the magnetic constant. To simplify the model and avoid solving the magnetostatic problem, we set $\mathbf{H} = \mathbf{H}_0$, so $\mathbf{L}_{mag} = \mu_0\,\mathbf{M}_r \times \mathbf{H}_0$. We assume that the residual magnetization is uniform, constant, and directed along the cantilever axis, since small magnetic fields are considered and NdFeB particles have large anisotropy.

2.3. Variational Formulation of the Problem

For the numerical solution of the boundary value problem, we present its variational formulation in the Lagrangian form, where the variable quantity is the displacement $\mathbf{u}$. To account for geometric nonlinearity, the strain tensor is defined as follows:

$$\mathbf{e} = \frac{1}{2}\left(\nabla\mathbf{u} + (\nabla\mathbf{u})^T + \nabla\mathbf{u}\cdot(\nabla\mathbf{u})^T\right).$$

To account for the rotation of the remanent magnetization vector $\mathbf{M}_r$ during bending of the plate, we introduce the rotation tensor $\mathbf{R}$ as follows:

$$\mathbf{R} = \mathbf{g} + \frac{1}{2}\left((\nabla\mathbf{u})^T - \nabla\mathbf{u}\right),$$

so that the magnetization after bending equals $\mathbf{R}\cdot\mathbf{M}_r$.

Let Ω_N and Ω_ε represent the regions occupied by titanium nickelide and the magnetoactive elastomer, respectively. The variational equation is written as follows:

$$\int_{\Omega_N}\left(2\,G_N(\varphi_M)\,(\mathbf{e}-\mathbf{e}_{Ph})\cdot\cdot\,\delta\mathbf{e} + \lambda_N(\varphi_M)\,I_1(\mathbf{e}-\mathbf{e}_{Ph})\cdot\cdot\,I_1(\delta\mathbf{e})\right)dV_N + \int_{\Omega_\varepsilon}\left(2\,G_\varepsilon\,\mathbf{e}\cdot\cdot\,\delta\mathbf{e} + \lambda_\varepsilon\,I_1(\mathbf{e})\cdot\cdot\,I_1(\delta\mathbf{e})\right)dV_\varepsilon - \int_{\Omega_\varepsilon}\mu_0\,\delta\mathbf{R}\cdot\mathbf{M}_r\cdot\mathbf{H}_0\,dV_\varepsilon. \quad (7)$$

This equation can be rewritten in dimensionless form:

$$\int_{\Omega_N}\left(2\,\overline{G}_N(\varphi_M)\,(\mathbf{e}-\mathbf{e}_{Ph})\cdot\cdot\,\delta\mathbf{e} + \overline{\lambda}_N(\varphi_M)\,I_1(\mathbf{e}-\mathbf{e}_{Ph})\cdot\cdot\,I_1(\delta\mathbf{e})\right)d\overline{V}_N + \int_{\Omega_\varepsilon}\left(2\,\mathbf{e}\cdot\cdot\,\delta\mathbf{e} + \overline{\lambda}_\varepsilon\,I_1(\mathbf{e})\cdot\cdot\,I_1(\delta\mathbf{e})\right)d\overline{V}_\varepsilon - \int_{\Omega_\varepsilon}\delta\mathbf{R}\cdot\overline{\mathbf{M}}_r\cdot\overline{\mathbf{H}}_0\,d\overline{V}_\varepsilon, \quad (8)$$

where the following dimensionless quantities are introduced:

$$\overline{G}_N(\varphi_M) = G_N(\varphi_M)/G_\varepsilon, \quad \overline{\lambda}_N(\varphi_M) = \lambda_N(\varphi_M)/G_\varepsilon, \quad \overline{\lambda}_\varepsilon = \lambda_\varepsilon/G_\varepsilon,$$
$$\overline{\mathbf{M}}_r = \sqrt{\mu_0/G_\varepsilon}\,\mathbf{M}_r, \quad \overline{\mathbf{H}}_0 = \sqrt{\mu_0/G_\varepsilon}\,\mathbf{H}_0,$$
$$d\overline{V}_N = dV_N/h^3, \quad d\overline{V}_\varepsilon = dV_\varepsilon/h^3.$$

2.4. Numerical Solution

The problem was solved numerically by the finite element method, implemented using an open computing platform for solving partial differential equations FEniCS [27]. The mesh covering the computational domain (the fragments of which are shown in Figure 2) consists of triangular elements and is generated automatically with specified parameters (with refinement near the titanium nickelide region—the lower part of the sample) using the gmsh package [28]. A linear approximation of the displacement vector $\mathbf{u}$ was used.

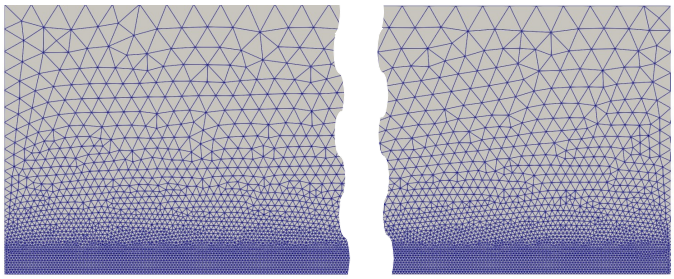

Figure 2. Fragments of the finite element mesh (**left** and **right** ends) with thickening in the titanium nickelide region.

To solve the variational problem (8), it is necessary to know the phase strains $\mathbf{e}_{Ph}$. Since Equations (3) and (4) are written for the increment of phase strains, the problem is solved using the step-by-step loading method: the entire cooling or heating process is divided into a series of small temperature steps, and at each step, the increment of the martensitic phase fraction and the phase strain increment are calculated. The total phase strains at each step are computed as the sum of the accumulated phase strains and the phase strain increment. The nonlinear variational equation (due to geometric nonlinearity) was solved by Newton's method using the FEniCS computing platform.

3. Results

For numerical simulation, the following parameter values were used for titanium nickelide (NiTi):

- Elastic moduli in the austenitic and martensitic states $\overline{E}_A = E_A/G_\varepsilon = 8.4 \cdot 10^4$, $\overline{E}_M = E_M/G_\varepsilon = 2.8 \cdot 10^4$, and Poisson's ratio $\nu = 0.3$;
- Temperatures for the start and finish of direct and reverse martensitic transformations $M_s = 313$ K, $M_f = 293$ K, $A_s = 323$ K, and $A_f = 343$ K (in our calculations, we do not account for the dependence of the critical transformation temperatures on material stresses);
- Material parameters associated with phase strain accumulation $\beta = 1.17 \cdot 10^{-3}$, $a_0 = 0.718$, $\bar{c}_0 = c_0$, and $G_\varepsilon = 0.283 \cdot 10^{-3}$;

Further, we use the following parameter values for the magnetoactive elastomer:

- The Lamé parameter $\overline{\lambda}_\varepsilon = \lambda_\varepsilon/G_\varepsilon = 100$;
- Residual magnetization $\overline{M}_r = \sqrt{\mu_0/G_\varepsilon}\, M_r = 0.275$.

For numerical calculations, the plate length was set to be 10 times its thickness ($l = 10\,h$).

Figure 3 shows the loading diagram of the bi-layer plate: during the first k steps, the magnetic field increases from $\overline{H}_0 = 0$ to $\overline{H}_0 = 0.1$ at a constant temperature $\Theta = 313$ K, corresponding to the austenitic state of titanium nickelide; over the next k steps, the temperature decreases to $\Theta = 293$ K, corresponding to the martensitic state of titanium nickelide, under a constant magnetic field of $\overline{H}_0 = 0.1$. Over the final k steps, the magnetic field is reduced to $\overline{H}_0 = 0$ at a constant temperature of $\Theta = 293$ K. Thus, the plate remains in the martensitic state with accumulated strains from the phase transition, while the external magnetic field is absent.

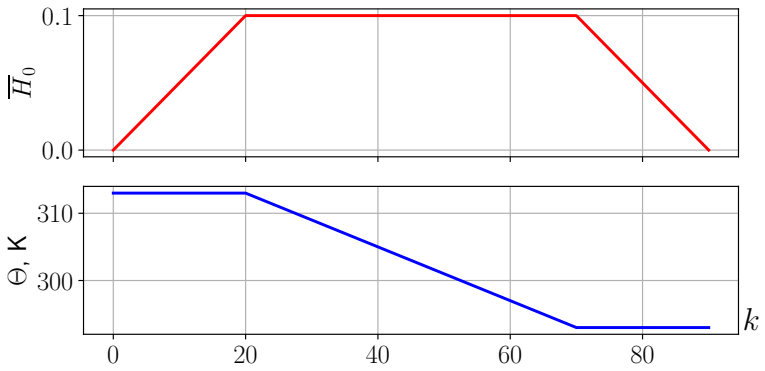

Figure 3. Loading diagram: dependence of magnetic field and temperature on step number k.

Figure 4 shows the following configurations of the plate: 1—initial configuration, 2—after application of the magnetic field, 3—after cooling under a constant magnetic field, and 4—after removal of the magnetic field (this configuration is determined by phase strains arising in titanium nickelide during the direct phase transition upon cooling). The color shows the distribution of the displacement vector component $\overline{u}_y = u_y/h$. These configurations were obtained for a titanium nickelide layer thickness of $\overline{h}_N = 0.1$.

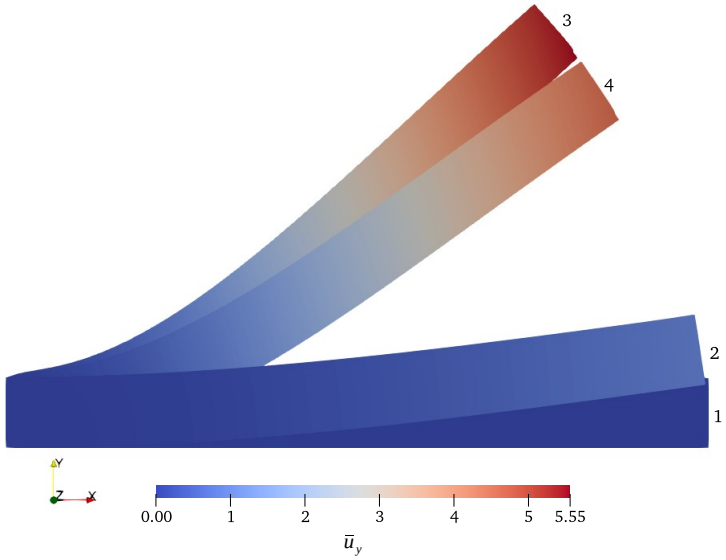

Figure 4. Configurations of the bi-layer plate: 1—initial configuration, 2—after application of the magnetic field, 3—after cooling under a constant magnetic field, and 4—after removal of the magnetic field.

When a magnetic field is applied along the y axis, the residual magnetization vector in the magnetoactive elastomer aligns with this field, causing the plate to bend and resulting in stress throughout the plate (in both the magnetoactive elastomer and titanium nickelide). Figure 5a shows the stress intensity distribution in the left part of the sample (maximum stresses occur closer to the fixed area). The phase strains arising in the titanium nickelide layer during cooling are proportional to the stresses. Figure 5b shows the axial component distribution of the phase strain tensor in the left part of the sample, with a maximum strain value of 1.6%. These strains determine the plate's bend magnitude after the magnetic field is removed. Note that if the plate is heated to a temperature at which titanium nickelide is in the austenitic state, the phase strains will completely disappear during the reverse phase transition and the sample will return to the initial configuration (configuration 1 in Figure 4).

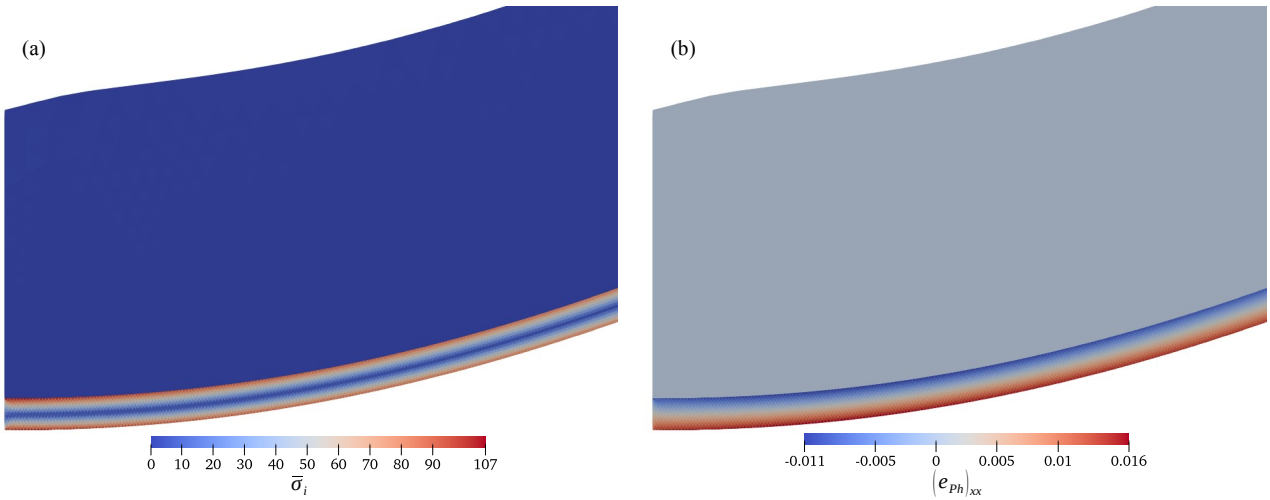

Figure 5. Stress intensity distribution (**a**) and phase strain distribution (**b**) in the left part of the sample.

It is evident that the plate's deflection magnitude (displacement of the right end $\overline{u}_y^{end} = u_y^{end}/h$ of the cantilever) will depend on the thickness of the titanium nickelide layer $\overline{h}_N = h_N/h$. Figure 6 shows the dependence of the deflection magnitude $\overline{u}_y^{end}$ on

step number k, corresponding to Figure 3, at various values of titanium nickelide layer thickness $\overline{h}_N$.

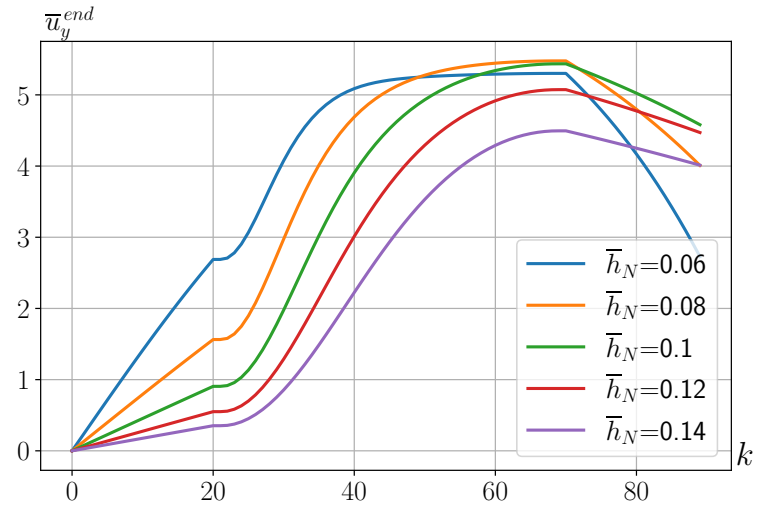

Figure 6. Dependence of the displacement of the right end of the cantilever on step number k for different values of the thickness of the titanium nickelide layer.

Figure 6 shows that the maximum deflection after plate cooling and after removal of the external magnetic field occurs at different titanium nickelide layer thicknesses $\overline{h}_N$, and these dependencies are generally non-monotonic. Figure 7 shows curves (deflection in the magnetic field—blue curve; deflection after the magnetic field is removed—red curve) from which one can find the values of $\overline{h}_N$ corresponding to maximum deflection in the magnetic field $\overline{H}_0 = 0.1$. For this field, the maximum free end displacement magnitude is $\overline{u}_y^{end} = 5.5$ at a titanium nickelide layer thickness of $\overline{h}_N = 0.088$ in the magnetic field and $\overline{u}_y^{end} = 4.6$ at a titanium nickelide layer thickness of $\overline{h}_N = 0.106$ after the magnetic field is turned off. Thus, the thickness of the titanium nickelide layer can be selected to achieve the required residual plate deflection.

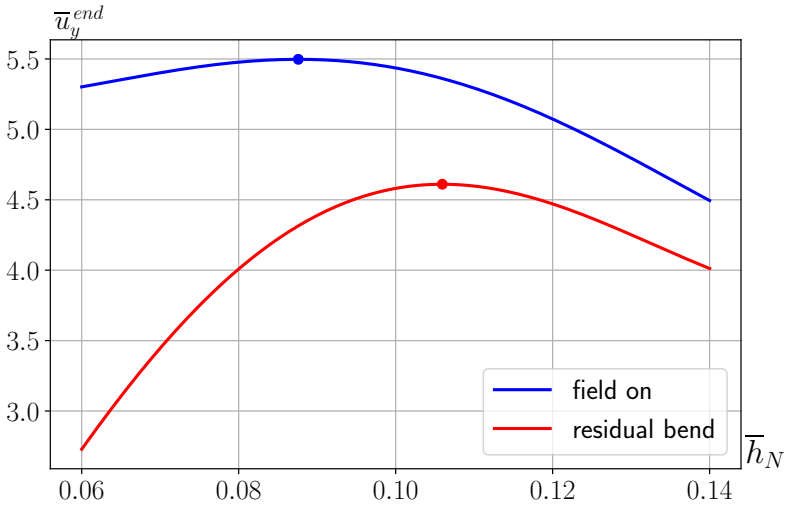

Figure 7. Dependence of the plate deflection magnitude on the thickness of the titanium nickelide layer.

The deflection magnitude of the bi-layer plate will depend not only on the thickness of the titanium nickelide layer but also on the magnitude of the magnetic field applied during the plate's bending. Figure 8 shows the dependence of the deflection magnitude (deflection in the magnetic field—blue curve; deflection after the magnetic field is removed—red curve)

on the magnitude of the applied magnetic field at a titanium nickelide layer thickness of $\overline{h}_N = 0.1$. From this figure, it can be seen that an increase in the magnetic field leads to an increase in the deflection, and this dependence is nonlinear. Using these dependencies, the magnetic field magnitude necessary to achieve a specified residual plate deflection can be determined. The difference between the displacement of the cantilever's free end before and after the magnetic field is removed also increases with an increase in the applied magnetic field.

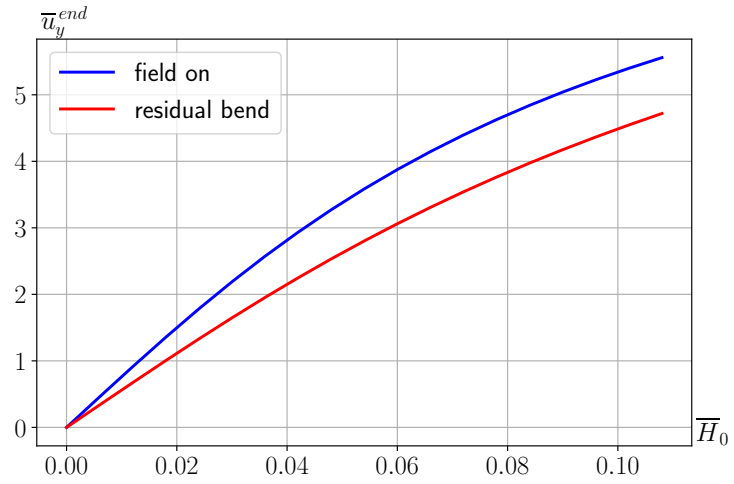

Figure 8. Dependence of the plate deflection magnitude on the applied magnetic field.

To check the convergence of the numerical method, we present a convergence plot for a series of numerical calculations with different numbers of mesh nodes. Figure 9 shows the dependence of the displacement vector norm $\|\overline{\mathbf{u}}\| = \left(\int_\Omega \overline{\mathbf{u}} \cdot \overline{\mathbf{u}}\, dV\right)^{1/2}$ on the number of mesh nodes N_{nodes}. This displacement is at the end point of the process under consideration (after removing the magnetic field). The ratio of the element sizes in the upper and lower parts remained 1 to 10. It is evident from the figure that with an increase in the number of nodes, the numerical solution reaches a constant value, which shows the convergence of the method.

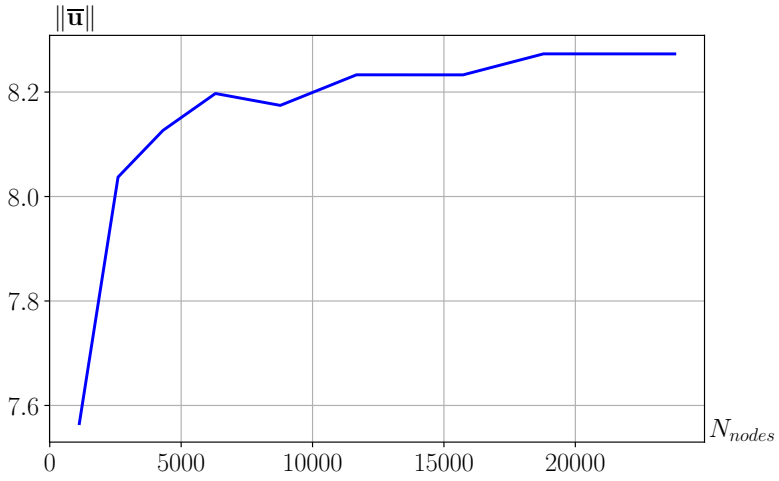

Figure 9. Dependence of the displacement vector norm on the number of mesh nodes.

4. Discussion

This study models the behavior of a cantilever (a bi-layer plate) composed of titanium nickelide (NiTi) and a magnetoactive elastomer containing magnetically hard NdFeB particles. The preliminary deflection is set as follows: in the high-temperature state (austenitic) for titanium nickelide, an external magnetic field is applied perpendicular to the cantilever

axis (and the residual magnetization vector in the MAE layer); then, the sample is cooled in such a way that a direct phase transition occurs in the titanium nickelide layer, after which the magnetic field is removed in the low-temperature state. It should be noted that titanium nickelide is in the martensitic state at room temperature. By switching the magnetic field on and off, the position of the cantilever's free end can be controlled.

The influence of the applied magnetic field magnitude and the thickness of the titanium nickelide layer on the cantilever deflection was investigated. The optimal NiTi layer thickness, which maximizes deflection (both before and after magnetic field removal), was identified. The dependence of the residual cantilever deflection on the lied magnetic field was obtained.

In order to understand whether it is possible to bend a real sample with a magnetic field, it is necessary to estimate the concentration of magnetically hard particles. For this, let us set $G_\varepsilon = 1$ MPa, which corresponds to realistic values for existing magnetoactive elastomers (MREs). Then, $M_r = 0.275\sqrt{G_\varepsilon/\mu_0} \approx 245$ kA/m. Given that the saturation magnetization of NdFeB particles is about 800 kA/m, this results in an approximate volume concentration of 30%. The dimensional value of the magnetic field is $H_0 = 0.1\sqrt{G_\varepsilon/\mu_0} \approx 90$ kA/m, which corresponds to moderate laboratory field strengths.

The results of this study make it possible to calculate the bi-layer cantilever's operation as an actuator, which can, for example, perform object gripping upon application of a magnetic field (when using two cantilevers). The required magnetic field strength to achieve a specified deflection can be determined (a preliminary deflection of the grip is created by applying a magnetic field in a high-temperature state, cooling to a low-temperature state, and then turning off the magnetic field), and the working displacement of the grip, defined by the difference in free-end movement before and after magnetic field removal, can be calculated. Figure 10 shows the working mechanism of such a gripper, consisting of a pair of bi-layer cantilevers with inner MAE layers and outer NiTi layers. In Figure 10a, the elements' position in the absence of a magnetic field is shown, while Figure 10b illustrates the position when the magnetic field is applied.

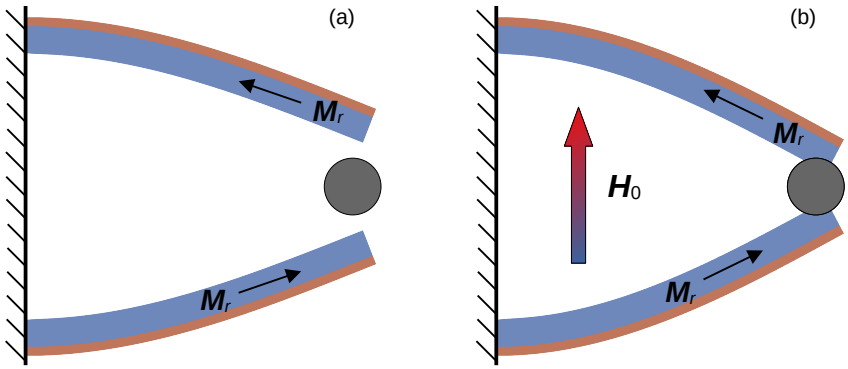

Figure 10. Working scheme of the gripper: element position in the absence of a magnetic field (**a**) and element position in a magnetic field (**b**).

Let us estimate the force that the gripper can implement when a magnetic field is applied. Here, we will not solve the contact problem in its full formulation; instead, after obtaining the preliminary deflection of the cantilever, we will assume that the boundary of the gripped object of length l_c coincides with the boundary of the cantilever and is located on the right edge (in the numerical calculation, displacements in the contact area are fixed). After applying the magnetic field, we integrate the stresses over the contact area and find the force. For $l_c = h = 0.5$ cm and $H_0 = 90$ kA/m, we obtain a force $F = 1.25$ N.

We also note that the cantilever could be a critical component in the following:

- Soft robotics: acts as a flexible gripper for fragile objects with variable stiffness, allowing for adaptive control.

- Medical devices: supports minimally invasive instruments that require precise manipulation in confined spaces, such as endoscopic actuators.
- Variable stiffness actuators: uses dual-stimulus control for complex programmable deformation profiles.

These examples highlight the versatility and practical relevance of the research.

The model presented in this study is relatively simple, yet it effectively describes the operation of the bi-layer cantilever. In the future, this model will be extended by defining constitutive relations within the framework of finite deformations. Additionally, a contact problem will be formulated and solved to simulate the operation of a gripper using a bi-layer cantilever as its element.

Author Contributions: O.S.S.: conceptualization, investigation, formal analysis, and writing—original draft preparation; O.V.S.: conceptualization, investigation, software, visualization, and writing—review and editing. All authors have read and agreed to the published version of the manuscript.

Funding: This work was funded by the Ministry of Science and Higher Education of the Russian Federation (theme No. AAAA-A20-120022590044-7).

Data Availability Statement: The original contributions presented in this study are included in the article. Further inquiries can be directed to the corresponding author.

Conflicts of Interest: The authors declare no conflicts of interest.

References

1. Wang, W.; Tang, Y.; Li, C. Controlling bending deformation of a shape memory alloy-based soft planar gripper to grip deformable objects. *Int. J. Mech. Sci.* **2021**, *193*, 106181. [CrossRef]
2. Tang, X.; Li, H.; Ma, T.; Yang, Y.; Luo, J.; Wang, H.; Jiang, P.A. Review of Soft Actuator Motion: Actuation, Design, Manufacturing and Applications. *Actuators* **2022**, *11*, 331. [CrossRef]
3. Teodoriu, A.P.; Pricop, B.; Lohan, N.M.; Popa, M.; Comăneci, R.I.; Doroftei, I.; Bujoreanu, L.G. Designing a Robotic Gripper Based on the Actuating Capacity of NiTi-Based Shape Memory Wires. *Actuators* **2024**, *13*, 319. [CrossRef]
4. Chung, H.J.; Parsons, A.M.; Zheng, L. Magnetically Controlled Soft Robotics Utilizing Elastomers and Gels in Actuation: A Review. *Adv. Intell. Syst.* **2021**, *3*, 2000186. [CrossRef]
5. Alexandron, I.; deBotton, G. Experimental Study of Nitinol Springs: Apparatus and Results. *Exp. Mech.* **2024**, *64*, 981–994. [CrossRef]
6. Böse, H.; Gerlach, T.; Ehrlich, J. Magnetorheological elastomers—An underestimated class of soft actuator materials. *J. Int. Mater. Syst. Struct.* **2021**, *32*, 1550–1564. [CrossRef]
7. Megginson, P.; Clark, J.; Clarson, R. Optimizing the Electrode Geometry of an In-Plane Unimorph Piezoelectric Microactuator for Maximum Deflection. *Modelling* **2024**, *5*, 1084–1100. [CrossRef]
8. Boyraz, P.; Runge, G.; Raatz, A. An Overview of Novel Actuators for Soft Robotics. *Actuators* **2018**, *7*, 48. [CrossRef]
9. Yao, D.R.; Heo, I.; Gao, W. Multimodal Soft Robotic Actuation and Locomotion. *Adv. Mater.* **2024**, *36*, 2308829. [CrossRef]
10. Xu, M.; Liu, Y.; Li, J.; Xu, F.; Huang, X.; Yue, X. Review of Flexible Robotic Grippers, with a Focus on Grippers Based on Magnetorheological Materials. *Actuators* **2024**, *17*, 4858. [CrossRef]
11. Qian, H.; Umar, M.; Khan, M.; Shi, Y.; Manan, A.; Raza, A.; Li, F.; Li, Z.; Chen, G. A state-of-the-art review on shape memory alloys (SMA) in concrete: Mechanical properties, self-healing capabilities, and hybrid composite fabrication. *Mater. Today Commun.* **2024**, *40*, 109738. [CrossRef]
12. Kim, M.S.; Heo, J.K.; Rodrigue, H.; Lee, H.T.; Pané, S.; Han, M.W.; Ahn, S.H. Shape Memory Alloy (SMA) Actuators: The Role of Material, Form, and Scaling Effects. *Adv. Mater.* **2023**, *35*, 2208517. [CrossRef] [PubMed]
13. Lucarini, S.; Hossain, M.; Garcia-Gonzalez, D. Recent advances in hard-magnetic soft composites: Synthesis, characterisation, computational modelling, and applications. *Compos. Struct.* **2022**, *279*, 114800. [CrossRef]
14. El-Atab, N.; Mishra, R.B.; Al-Modaf, F.; Joharji, L.; Alsharif, A.A.; Alamoudi, H.; Diaz, M.; Qaiser, N.; Hussain, M.M. Soft Actuators for Soft Robotic Applications: A Review. *Adv. Intell. Syst.* **2020**, *2*, 2000128. [CrossRef]
15. Lagoudas, D.C. *Shape Memory Alloys. Modeling and Engineering Applications*; Springer Science+Business Media: New York, NY, USA, 2008. [CrossRef]
16. Mashikhin, A.E.; Movchan, A.A. Problem of direct martensite transformation in a thick-walled cylinder made of shape memory alloy. *Mech. Solids* **2016**, *51*, 321–333. [CrossRef]
17. Becker, T.I.; Stolbov, O.V.; Biller, A.M.; Borin, D.Y.; Stolbova, O.S.; Zimmermann, K.; Raikher, Y.L. Shape-programmable cantilever made of a magnetoactive elastomer of mixed content. *Smart Mater. Struct.* **2022**, *31*, 105021. [CrossRef]

18. von Lockette, P.; Lofland, S.E.; Biggs, J.; Roche, J.; Mineroff, J.; Babcock, M. Investigating new symmetry classes in magnetorheological elastomers: Cantilever bending behavior. *Smart Mater. Struct.* **2011**, *20*, 105022. [CrossRef]
19. Borin, D.Y.; Stepanov, G.V.; Odenbach, S. Tuning the tensile modulus of magnetorheological elastomers with magnetically hard powder. *J. Phys. Conf. Ser.* **2013**, *412*, 012040. [CrossRef]
20. Zhao, R.; Kim, Y.; Chester, S.A.; Sharma, P.; Zhao, X. Mechanics of hard-magnetic soft materials. *J. Mech. Phys. Solids* **2019**, *124*, 244–263. [CrossRef]
21. Durastanti, R.; Giacomelli, L.; Tomassetti, G. Shape programming of a magnetic elastica. *Math. Model. Methods Appl. Sci.* **2021**, *31*, 675–710. [CrossRef]
22. Rogovoi, A.A.; Stolbova, O.S. Modeling elastic-inelastic processes in shape memory alloys at finite deformations. *J. Appl. Mech. Tech. Phys.* **2013**, *54*, 295–307. [CrossRef]
23. Kumbhar, S.B.; Chavan, S.P.; Gawade, S.S. Adaptive tuned vibration absorber based on magnetorheological elastomer-shape memory alloy composite. *Mech. Syst. Signal Process.* **2018**, *100*, 208–223. [CrossRef]
24. Movchan, A.A.; Shelymagin, P.V.; Kazarina, S.A. Constitutive equations for two-step thermoelastic phase transformations. *J. Appl. Mech. Tech. Phys.* **2001**, *42*, 864–871. [CrossRef]
25. Landau, L.D.; Lifshitz, E.M. *Theory of Elasticity*; Butterworth-Heinemann: Oxford, UK, 1986.
26. Lurie, A.I.; Belyaev, A. *Theory of Elasticity*; Springer: Berlin/Heidelberg, Germany, 2005. [CrossRef]
27. FEniCS Computing Platform. Available online: http://www.fenicsproject.org (accessed on 31 October 2024).
28. Gmsh Package. Available online: http://www.gmsh.info (accessed on 31 October 2024).